A miniature and intelligent Low-Power in situ wireless monitoring system for automotive wheel alignment

Xiaoli Tang [a,c], Yu Shi [b], Boyue Chen [b], Mark Longden [c], Rabiya Farooq [c], Harry Lees [a,c], Yu Jia [a,*]

[a] *School of Engineering and Technology, Aston University, Birmingham B4 7ET, UK*
[b] *Smart Composite Group, University of Chester, Chester CH1 4BJ, UK*
[c] *RL Automotive, Trident Business Park, Unit 5C, Basil Hill Rd, Didcot OX11 7HJ, UK*

ARTICLE INFO

ABSTRACT

Automotive wheel misalignment is the most significant cause of excessive wear on tires, which will severely affect the stability and safety of vehicle handling, and cause serious consequences for human health and the environment. In this study, an energy-efficient onboard wheel alignment wireless monitoring system (WAWMS) is developed to detect wheel misalignment in real time. To minimise power consumption, a dual wake-up strategy is proposed to wake the microcontroller by a real-time clock (RTC) and an accelerometer. Furthermore, an online self-calibration method of inertial measurement unit (IMU) sampling frequency is investigated to improve measurement accuracy. Eventually, real-world wheel misalignment tests were performed with the WAWMS. The error-correcting output codes based support vector machines (ECOC-SVM) method successfully classifies different wheel alignment conditions with an average accuracy of 93.2% using nine principal components (PCs) of 3-axis acceleration spectrum matrixes. It validates the effectiveness of the designed WAWMS on automotive wheel alignment monitoring.

1. Introduction

Camber, caster and toe are three primary alignment angles of vehicle wheels [1]. They regulate the positions of wheels relative to the suspension and the ground. Camber and toe angles are related to the wheel orientation, while the caster is a measurement of the suspension geometry. Misalignment of vehicle wheels, especially titled toe angles, will cause severe uneven and excessive surface wear of tires, roads and other suspension components. This not only increases fuel and/or electricity costs but also affects the stability and safety of vehicle steering and handling [2]. More importantly, harmful particulate matter (PM) emissions caused by tire wear have a serious and noticeable impact on human health and the environment. Therefore, four-wheel alignment including correct inspection and adjustment of the characteristic angles is significantly essential [3].

Currently, commercial wheel alignment inspection and correction is carried out offline by means of expensive specialist equipment and advanced alignment technology at the service centre, which is a time-consuming and laborious process. Generally, vehicle owners or operators are advised to send their vehicles for proactive maintenance frequently to correct wheel alignment. Currently, researchers are mainly committed to the investigation of alignment techniques to improve calibration precision and speed during maintenance. Most existing wheel alignment measurements are carried out with expensive machine vision equipment. For example, more than 300 wheel alignment measurements were performed by Patel *et al.* [4] to capture the effects on static wheel alignment accuracy. The test results showed that both platform levelness and tire pressure errors significantly affected the wheel alignment accuracy. Furferi *et al.* [5] and Padegaonkar *et al.* [6] developed 3D machine vision-based systems for contactless measurement of wheel alignment respectively, which were effectively validated by measuring toe and camber angles. Shao *et al.* [7] designed a new type of four-wheel calibration device driven by three motors to accurately calibrate four-wheel alignment parameters. Furthermore, they proposed a local fractal dimension analytical method relying on blanket technology to optimize the measurement range to avoid repetitive large-scale computations during the estimation of alignment parameters [8]. Kim *et al.* [9] investigated a quick, reliable and cost-efficient wheel alignment inspection approach for automakers by employing two laser modules and several jigs to measure the toe and camber angles for the suspension module. Its accuracy was compared and validated with the results of the vision system with two CMOS cameras. Niu *et al.* [10] developed an analytical assembly variation analysis method based on

Nomenclature

ACC	accelerometer
ADC	analogue to digital converter
ECOC	error-correcting output codes
FFT	fast Fourier transform
FIFO	first in first out
GPIO	general-purpose input/output
HGV	heavy goods vehicle
IMU	inertial measurement unit
IoT	Internet of things
MCU	microcontroller unit
MEMS	micro-electromechanical systems
PC	principal component
PCA	principal component analysis
PDF	probability density function
PM	particulate matter
RTC	real-time clock
SVM	support vector machines
TPMS	tire-pressure monitoring system
WAWMS	wheel alignment wireless monitoring system
WDT	waterdog timer

Fig. 1. Different wheel alignment conditions.

equilibrium equations of incremental forces applied for 3D suspension systems, which was validated to be effective for the accurate control of wheel alignment parameters with the simulated model.

Generally, wheel misalignment is mainly caused by sudden impact or wear of suspension parts of vehicles, especially those heavy goods vehicles (HGVs). It occurs at any time so that is difficult or even impossible to immediately or punctually predict and maintain unless regular and periodic inspection for customers [1]. Therefore, it is essential to develop an onboard system for condition-based preventive maintenance to reduce the probability of failure and cost and improve safety. Additionally, these types of wireless sensing systems can reduce the cost and complexity of wheel misalignment detection operations. The continuously measured data can be uploaded to the cloud platform in real time for storage, management, and processing with predictive and prescriptive machine learning modelling to achieve the auto-align system. When the misalignment occurs or is imminent, the platform can inform and remind the driver in time to perform preventative maintenance to reduce the fuel cost, uneven tire wear, PM emissions and enhance the stability and safety of vehicle handling and steering. The conventional tire-pressure monitoring system (TPMS) as the onboard system has been broadly applied in commercial vehicles to continuously measure the wheel tire pressure status. Recently, the promising intelligent tire embedded with multiple sensors is drawing the attention of both researchers and automakers because of the increasing demand within the automotive industry for progressively safer vehicles [11].

Basically, the vibration responses captured by the sensing unit come from the excitation of the road and axle via the tyre and rim. The excitation from roads is a broadband source, which can be represented by the road power spectrum density. As shown in Fig. 1, different wheel misalignment cases have different angles with respect to the road excitation, which can be considered as the change of input. The alignment conditions also change the slip angle and slip ratio which are the variation of the transmission system [12]. The input and transmission system vary with the alignment conditions and consequently, the responses contain the information of the wheel alignment conditions. Accordingly, few researchers explore the possibilities of developing onboard wireless wheel alignment inspection systems with micro-electromechanical systems (MEMS) to continuously measure the automotive wheel alignment status from the viewpoint of dynamics [13]. For example, Sonali [12] designed a wireless sensing system utilising an accelerometer to measure
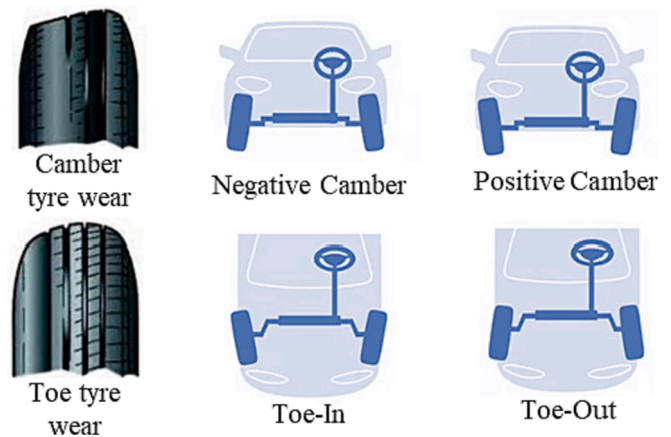
the automobile wheel parameters, including camber and toe. Michael and Isaac [14] integrated an automotive wheel alignment system with MEMS components with the power consumption of about 185mW and 727mW in idle and active modes, respectively. Young *et al.* [3,15] employed a 3-axis MEMS accelerometer and a MEMS gyro to capture signals from wheels to implement camber angle and toe angle inspection based on a microcontroller unit (MCU). The proposed calibration approach achieved a precision of low to $\pm 0.015°$. Liu *et al.* [16] applied MSP430 as the microcontroller to realize data communication between a two-axis inclination sensor and a hand-held terminal to effectively assist the four-wheel alignment. Paudel *et al.* [17] implemented sensorless detection of wheel alignment error for a wheeled mobile robot by a disturbance observer. The wheel torque profiles detected by the motor current were analysed and it was demonstrated that they were effective and efficient to detect camber or toe errors. Mohamad *et al.* [18] built a portable IoT based wheel alignment monitoring system and graphical user interface to perceive the customers' early detection of misalignment issues. D'Mello *et al.* [1] designed an IoT based wheel alignment system with an MPU6050 and an ESP32 microcontroller to detect the camber and toe angles.

However, because of the burdensome tasks (including collecting, storing, processing, and transmitting numerous datasets) of the MCU, the biggest challenge for the wireless sensor node is the extremely high demand for battery capacity, especially when it works in a harsh environment. In general, to prolong the service life of the wireless sensor node, there are two effective solutions: reducing power consumption [19] and energy harvesting [20,21]. Although energy harvesting can prolong the service life of the wireless sensor nodes, the energy harvested in harsh areas or environments is very limited. Therefore, the primary priority is to reduce the power consumption of the nodes, which provides a prospect of autonomous wireless alignment detection systems with the prospective assistance of energy harvesting [22] in the future. This would enable the sensor node to be widely used in other forthcoming applications as well, like rotating machinery monitoring in various industrial fields [23]. Some researchers commit to improving the power efficiency of the components, such as reducing the power consumption in broadcast, radio transmission and reception. It is important to reduce the instantaneous power of the components, but if the components always work, the average power consumption will undoubtedly increase. Consequently, making them enter the sleep modes is an optional approach. To automatically wake up the processor from system off mode, researchers commonly use wake-up methods including wake-up radio [24,25], timers or clocks [26], accelerometers [27] and so on. However, it requires collecting valid dynamic signals for wheel alignment monitoring, and a single wake-up method is difficult to meet the requirements. Therefore, a low-power and efficient onboard wheel alignment wireless monitoring system with a dual wake-up strategy and

adaptive self-calibration is developed to achieve long-term online alignment monitoring of automotive steering axle wheels in this study. The main contributions of this article include:

1) An efficient dual wake-up strategy is proposed to not only prolong the service life of the designed WAWMS but also guarantee the validity of the collected data for wheel alignment monitoring.
2) An online adaptive self-calibration method of IMU sampling frequency is investigated with the recorded data packet time duration to alleviate the measurement uncertainty and improve the sensor accuracy.
3) Some wheel misalignment experiments were carried out with the designed WAWMS in the field, and the ECOC-SVM method was applied to the collected data to demonstrate the effectiveness and efficiency of WAWMS in wheel alignment monitoring.
4) An energy-efficient onboard WAWMS is designed and manufactured to monitor the condition of automotive wheel alignment in real time, and its power consumption is analysed at entire working stages. It has great potential to substitute for the conventional TPMS and can be versatile in condition monitoring of automotive.

The rest of this paper is arranged as follows. Section 2 describes the design and integration of the WAWMS, and then introduces the proposed dual wake-up strategy to reduce the average power consumption. Section 3 analyses the power consumption of the integrated WAWMS. Section 4 proposes an effective and adaptive online self-calibration method for the sensor sampling rate. In Section 5, the wheel misalignment experimental studies were performed and the captured measurements are analysed to demonstrate the effectiveness and efficiency of the designed WAWMS. Finally, conclusions and future work are presented.

2. WAWMS and power management

2.1. WAWMS design and integration

A peripheral device generally refers to a wireless sensor node that consists of a sensing unit, a power unit, an MCU and a communication unit. The sensing unit generally contains one or more sensors to sense the physical characteristics of the target object. The power unit normally includes a power supply battery or an energy harvesting device and a power management module, such as regulators. The MCU is the core of the overall system, which is responsible for the communication between different units, as well as the storage and processing of datasets, etc. Finally, the captured measurements or extracted features can be sent to the central devices by the communication unit, such as Wi-Fi, Bluetooth, Zigbee and 4G/5G modules and so on. According to the basic structure of a wireless sensor node, a WAWMS was designed with the architecture

shown in Fig. 2. It primarily consists of a battery, a buck converter, a battery voltage monitoring module, a powerful MCU, a Bluetooth 5 transmitter with an internal printed circuit board (PCB) antenna, a 9-DOF IMU, a temperature and pressure sensor, an RTC and a 3-axis accelerometer (ACC) used for the proposed dual wake-up strategy.

The red and blue lines with arrows represent the power supply directions and communication between different modules, respectively. The framework apparently shows that only the battery voltage monitoring module and the buck converter are directly powered by the battery. The battery voltage monitoring module can test the battery voltage in real time, which will be helpful to remind the customer to replace the battery before it is fully depleted. Then, the buck converter converts the battery voltage into a fixed DC voltage to power the MCU and the Bluetooth, the RTC and the accelerometer modules to make them work smoothly and stably. The IMU, temperature and pressure sensor are powered from a general-purpose input/output (GPIO) port of the MCU unit because the output voltage can be driven by the MCU based on the requirement of the loads to reduce the average power consumption of the entire system. On the other hand, the RTC and the accelerometer must always be powered by the output voltage of the buck converter according to the effective dual wake-up strategy proposed to wake the MCU from sleep mode. If these modules or loads are directly powered by the battery, there will be two issues. Firstly, when the powered modules or loads generate a relatively large current, the battery voltage will sharply drop, which will seriously affect the performance of the load device or produce significant noise interfaces, especially for sensors. Secondly, since different modules have different operating power voltage requirements, the improper battery voltage may lead to the low energy efficiency of certain modules.

For the communication among different modules, the MCU reads the battery voltage measurements from an analogue input GPIO pin to monitor the voltage of the battery to alert the customer when the battery is nearly exhausted. Similarly, after the IMU and the temperature and pressure sensor record the signal profile, it is transferred to the MCU through the serial communication protocol, i.e. I2C or SPI, for storage and wireless transmission. However, advertisement, data collection and transmission consume a lot of power due to long working hours even though lots of researchers are devoted to the study of improving efficiency and reducing power consumption of electronic components. Therefore, when all datasets are successfully transmitted or when the vehicle operating condition does not meet the criteria for quality data collection, the system should enter a deep sleep mode to reduce power consumption. Correspondingly, a wake-up strategy is required to wake up the MCU under appropriate circumstances so that the WAWMS can collect and transmit sensing measurements effectively.

In order to reduce the dimensions of the designed WAWMS board, all components were selected and placed in a compact overall footprint on a
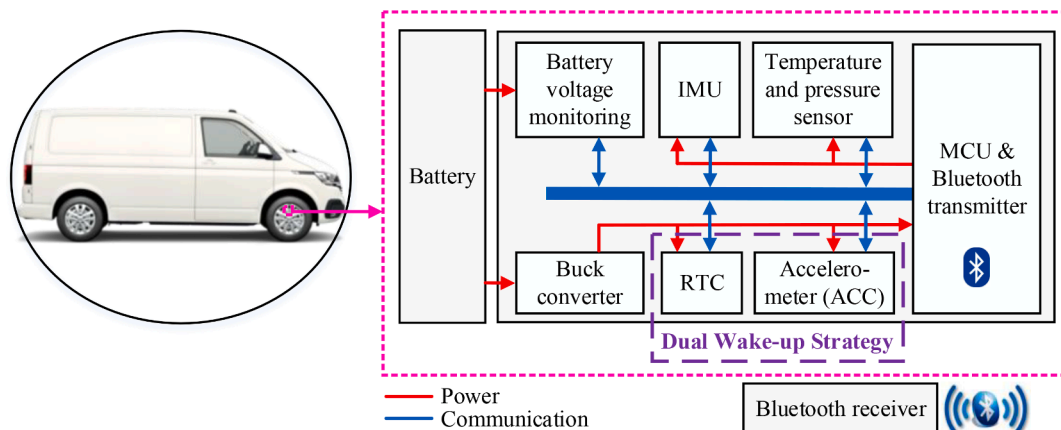

Fig. 2. Architecture of the designed wheel alignment wireless monitoring system.

multi-layer PCB. The requirements and advantages of the selected components are summarized in Table 1. An integrated WAWMS is shown in Fig. 3 (a). Its dimensions including low cost, low power, high performance, compact dimensions, and appropriate functionality are only 34.40*13.60*4.34 mm which is given in Fig. 3 (b).

2.2. Proposed dual Wake-up strategy

The MCU of the peripheral device should automatically switch between the working state and the sleep mode according to certain rules to reduce the power consumption of the peripheral device of the WAWMS while ensuring operating performance. Contrastly, the central device does not experience the same trade-off constraints between power consumption and operating performance as the peripheral device. Considering the automotive application, a dual wake-up strategy is proposed to alternately wake the system from deep sleep according to the interrupt signals generated by an external accelerometer and an RTC which are framed with the purple dashed line in Fig. 2 (a). Simultaneously, a soft reset of the system was set to prevent the system from hanging or freezing.

Firstly, since the collected data is useless when the vehicle is stationary or at a very low speed, it is necessary to wake up the system for sampling by the accelerometer when the vehicle speed is appropriate. Fig. 4 illustrates the acceleration analysis at the sensor installation position (the blue dot) on the vehicle wheel to induce the wake-up mechanism by the accelerometer. The radius of the tire and the distance from the sensor installation position to the centre of the tire are R and r, respectively. When the vehicle runs, the wheel rotates around the centre O at an angular velocity ω. The rotation angle is θ. A 3-axis accelerometer is installed in the X and Y directions to sense the

centrifugal acceleration a_c and the tangential acceleration a_t together with the components of gravity g, i.e. g_x and g_y, on these two axes. The centrifugal acceleration a_c is given as

$$a_c = \omega^2 r = (2\pi f)^2 r \tag{1}$$

where f is the rotating frequency of the wheel. The linear velocity v of the vehicle can be expressed as

$$v = \omega R = 2\pi f R \tag{2}$$

Therefore, the acceleration, a, measured by the accelerometer on the X-axis is calculated in (3).

$$a = a_c - g_x = (2\pi f)^2 r - g \bullet sin\theta = (v/R)^2 r - g \bullet sin\theta \tag{3}$$

As R, r and g are constant, and the rotation angle θ is regarded as changing within the range of $[0, 2\pi]$, the acceleration a changes within $\left[(v/R)^2 r - g, (v/R)^2 r + g\right]$. Therefore, the acceleration threshold can be set to be or a little lower than $(v/R)^2 r - g$, and the corresponding vehicle speed threshold is v. When the vehicle speed reaches the set threshold and lasts for a set duration of seconds, the accelerometer will generate an interrupt signal, which can successfully wake the MCU through a GPIO port. Then the sensors are powered to collect wheel alignment characteristics and transmit them to the central device. After that, the MCU will enter deep sleep mode again.

Furthermore, the MCU can be awakened by another interrupt signal generated by the RTC when the countdown timer or the alarm timing ends. The interrupt signal is a falling edge trigger that will be efficient and effective to reduce power consumption and prevent the wake-up behaviour continuously triggered by the accelerometer during the running of the vehicle. With this proposed dual wake-up strategy, the designed WAWMS will be more suitable for actual application scenarios because it not only effectively prevents repeated and meaningless sampling, such as when the vehicle is stationary or running at low speed, but also prominently prolongs the service life of the WAWMS. The workflow of the designed WAWMS is illustrated in Fig. 5.

The peripheral effectively works with the proposed dual wake-up strategy and follows the steps shown in Fig. 5. Once the peripheral device is powered or reset, the MCU sets two essential parameters according to the vehicle speed for the accelerometer, i.e. acceleration threshold and duration. It then enters the deep sleep mode to save power, leaving only the accelerometer to monitor the speed of the vehicle. Once the acceleration exceeds the threshold for a defined duration, an interrupt signal is generated by the accelerometer to wake the MCU from the deep sleep state. Synchronously, the interrupt signal and accelerometer settings are cleared to stop the vehicle speed monitoring. After that, the MCU sends instructions to request the sensors to complete the data collection tasks after confirming a successful connection with the central device. The collected datasets are sent back to the MCU through I2C/SPI and packaged for transmission to the central device via Bluetooth. For better power management, the MCU will go to the deep sleep state again after setting and enabling a countdown timer or an alarm timer by the RTC. An interrupt signal generated as the countdown timer or the alarm timer event can trigger the MCU to wake up to set parameters for the accelerometer, which can prevent the MCU from being needlessly awakened by the accelerometer interruption from a moving vehicle. This is the energy-efficient working cycle of the peripheral.

On the central side, the data packets can be received by the designed Bluetooth receiver or any portable device, like laptops, smartphones, and tablets. Finally, they will be transmitted to the cloud for storage and further analysis.

3. Power consumption of the WAWMS

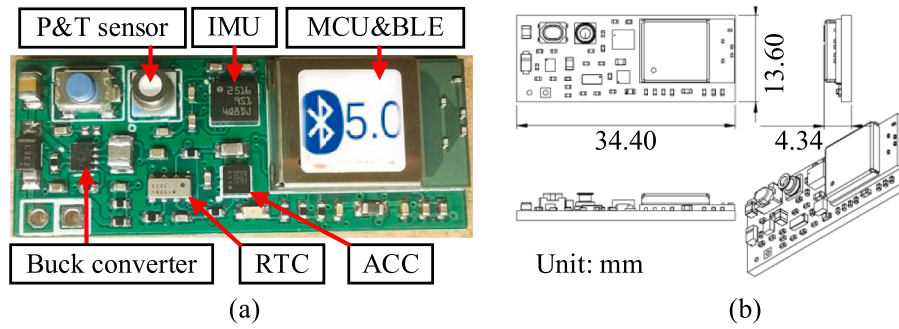To validate the effectiveness of the proposed dual wake-up strategy

Table 1
Requirements and advantages of selected components.

Components	Requirements and Advantages
Buck Converter	• Ultra-low power (60nA operating quiescent current) and low cost • Suitable input (1.8 V to 6.5 V) and output voltage ranges (selectable output voltage) • High conversion efficiency (80 % efficiency at the output current of 1uA) • Tiny dimensions (2 mm × 1.5 mm × 1 mm)
MCU and BLE	• Low power (0.4µA@3V in System OFF mode, no RAM retention) and low cost • High control and signal processing capabilities (ARM Cortex-M4 32-bit processor with FPU, 64 MHz) • Compact structure, tiny dimensions (11.6 mm × 10.0 mm × 2.23 mm) with an internal PCB antenna
9-DOF IMU	• High performance (embedded FIFO, 16-bit data output. etc.), compatibility, sample rate (up to 952 Hz), resolution and wide measurement range • Low power (operating mode down to 1.9 mA) and low cost • Compact and tiny dimensions
Pressure and Temperature	• Relatively high accuracy and resolution (1.57 mbar, 0.0086 °C) • Low power (down to 0.6µA) and low cost Ultra-small dimension (3.3 mm × 3.3 mm × 2.75 mm) • Better with a water-resistant package

RTC	• Ultra-low power (down to 45nA) and low cost
	• High accuracy (Factory calibrated: ±1 ppm, 32.768 kHz XTAL oscillator: ±5 ppm)
	  With the interrupt function
	  High compatibility and tiny dimensions (3.2 mm × 1.5 mm × 0.8 mm)

Accelerometer	• Ultra-low power (down to 2µA) and low cost • With the interrupt function and wide measurement range (±2g/±4g/±8g/±16 g dynamically selectable full scale) • Tiny dimensions (3 mm × 3 mm × 1 mm)

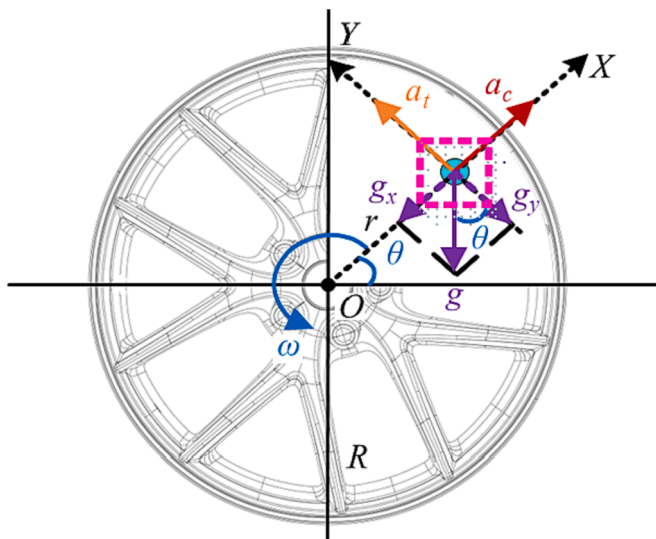**Fig. 3.** Designed WAWMS: (a) PCB board, and (b) dimensions.

Fig. 4. Component analysis of wheel acceleration.

in terms of low power consumption of the system, the power consumption of the integrated system is analysed under different working conditions in this section.

3.1. Power consumption analysis

Duty cycle and current in various activities and sleep states were recorded by Analog Discovery 2. Since some commonly used rechargeable lithium-ion batteries have a nominal voltage of 3.7 V, the experiments were carried out at a voltage of 3.7 V. A full duty cycle and its average current cost under different operating states are analysed and marked in Fig. 6.

The highest current is drawn during data collection. After data transmission and BLE disconnection, the MCU enables the RTC and enters the deep sleep state. In the sleep state, the WAWMS consumes as low as 9.13μA. The MCU is awakened by the interrupt signal generated when the RTC countdown ends. It is followed by disabling the RTC and enabling the accelerometer. Following this sequence, the MCU enters deep sleep again with the current consumption of only 10.46μA.

The input voltage range of the selected buck converter is from 1.8 V to 6.5 V, and its output voltage is from 1.8 V to 3.3 V in 100-mV steps. Because the supply voltage range of each component is different, the influence of the input and output voltages of the buck converter on the average current consumption of the designed WAWMS under different working conditions is analysed and compared in Fig. 7. For the buck converter, the input voltage supplied by an adjustable DC power supply station is changed from 2.25 V to 6.5 V, and the output voltage V_{OUT} is set to 2.3 V, 2.5 V, 2.8 V, 3.0 V and 3.3 V successively to implement the high performance of the components.

When the input voltage is slightly lower than the output voltage, the buck converter still operates but the stability and reliability of
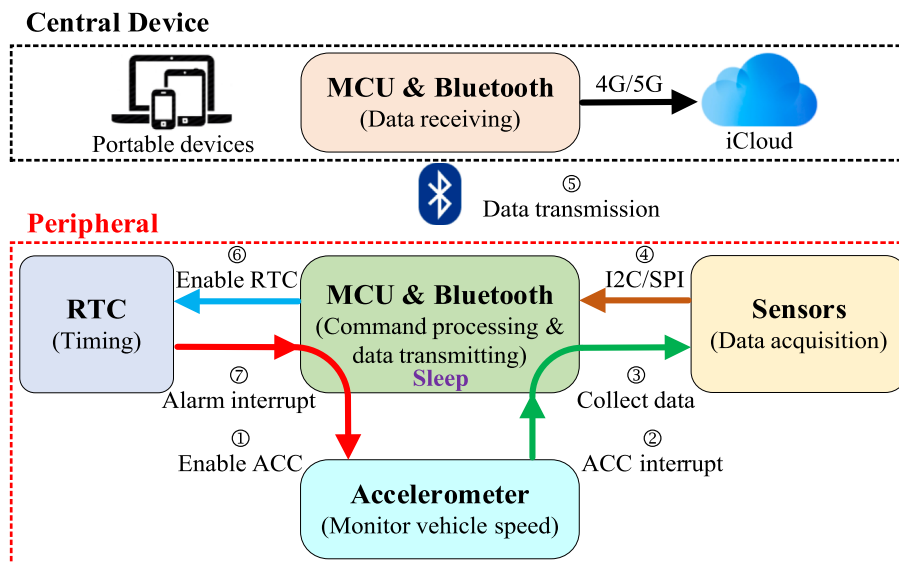

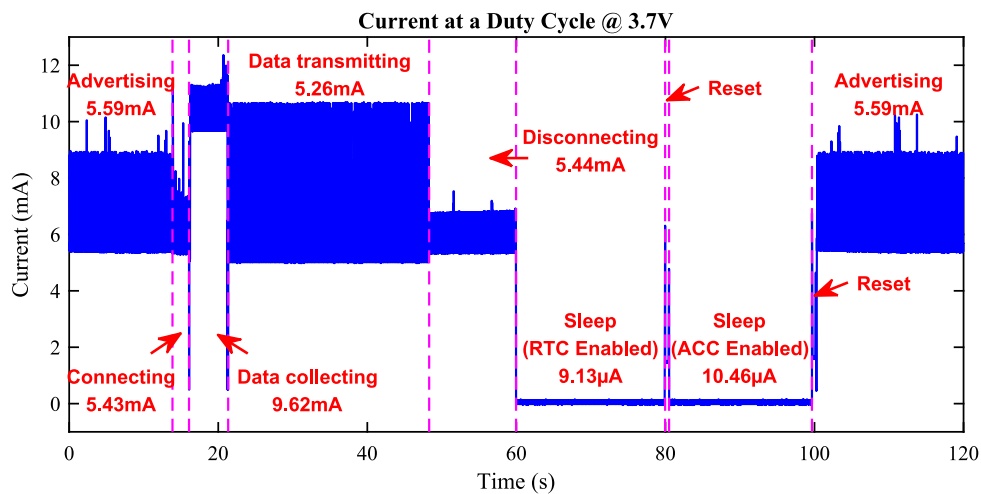**Fig. 5.** Workflow of the designed WAWMS.

Fig. 6. The current of the WAWMS under different operating states at the voltage of 3.7 V.
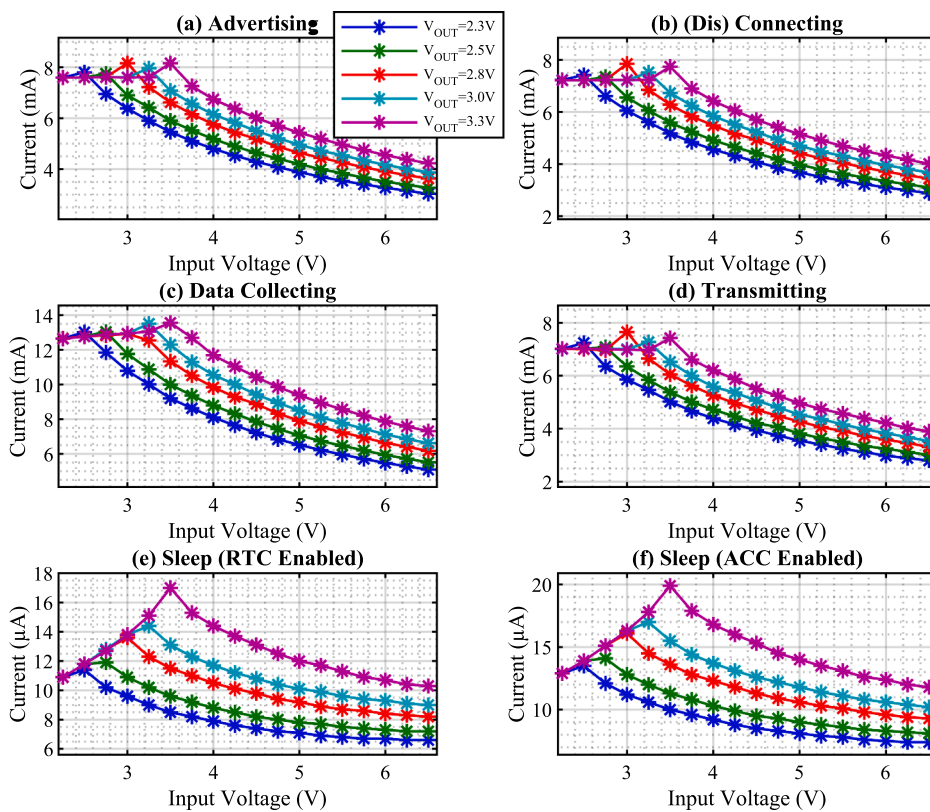

Fig. 7. Influence of the input and output voltages of the buck converter on current under various working conditions.

performance are sporadic. In the normal operating range with output voltage constant, the current drawn by the electrical components decreases with an increase in input voltage. Conversely, when the input voltage is constant, the current drawn increases with the output voltage rising. Consequently, considering the gradually decreased battery voltage and the trade-off between performance and current consumption, 2.5 V is selected as the output voltage of the buck converter in this design. Fig. 8 presents the current change trends under various working conditions at the output voltage of 2.5 V as the battery voltage drops from 6.5 V to 2.0 V in 0.25 V steps. The current consumption of the designed WAWMS is very low, especially in the deep sleep mode.

3.2. Comparison of power Consumption: A hypothetical case study

To illustrate the superiority of the proposed dual wake-up strategy in terms of power consumption and application, it is compared with the other three working modes: idle with a waterdog timer (WDT) enabled, sleep with RTC enabled, and sleep with accelerometer enabled. Suppose the MCU collects data for 5.042 s after being awakened. The related working conditions, current consumption and working periods are listed in Table 2.

To estimate the battery life of the WAWMS device, a hypothetical case study is set up using several well-founded assumptions. According to the EU regulations on driving hours, the maximum driving time cannot exceed 9 h a day. In addition, a break or breaks totalling at least
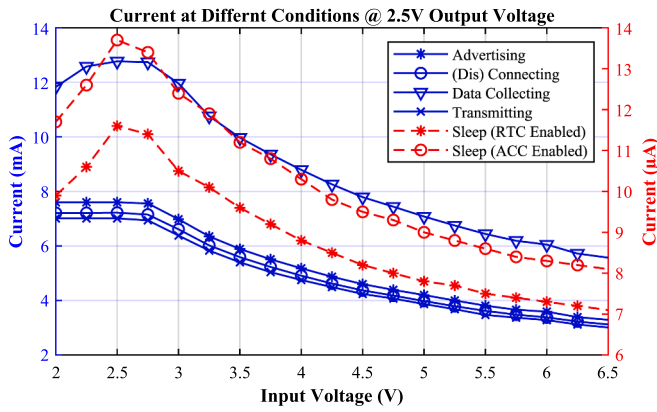
Fig. 8. Current change trends under various working conditions with different input voltages of the buck converter.

Table 2
Current and duration at various conditions in a working cycle @ V_{IN} = 3.7 V, V_{OUT} = 2.5 V.

Working Conditions	Current (mA)	Duration (s)
Advertising	5.59	60.0
Connecting	5.43	2.5
Data Collection	9.62	5.0
Transmitting	5.26	27.0
Disconnecting	5.44	11.8
Idle (WDT Enabled)	0.43	–
Sleep (RTC Enabled)	$9.13*10^{-3}$	–
Sleep (ACC Enabled)	$10.46*10^{-3}$	–

45 min are required after every 4 h 30 min driving interval. A 24-hour timeline is given in Fig. 9. An assumption is made that the driver starts driving at 9:00 for 4 h. The driver stops for a 1-hour break in-between and then continues to drive for another 4 h. With these assumptions, the driver works for 8 h a day and will complete the workday at 18:00. The working cycles within 24 h of four different working modes are displayed below the timeline in Fig. 9.

For Mode 1, when the MCU has no task, it enables the WDT and enters the idle state. The countdown time is set to 4 h. Once the countdown is over, a timeout signal will be generated to restart the MCU. Then, the sensor starts to collect data regardless of the current state of the vehicle. Mode 2 is like Mode 1, the difference is that when the MCU is idle, it will enter the deep sleep mode and only wake up by an interrupt signal generated by the RTC. In Mode 3, the accelerometer interrupt will be enabled before the MCU enters deep sleep. Once the vehicle speed exceeds the set threshold and lasts for a set duration, an interrupt signal generated by the accelerometer will wake up the MCU.
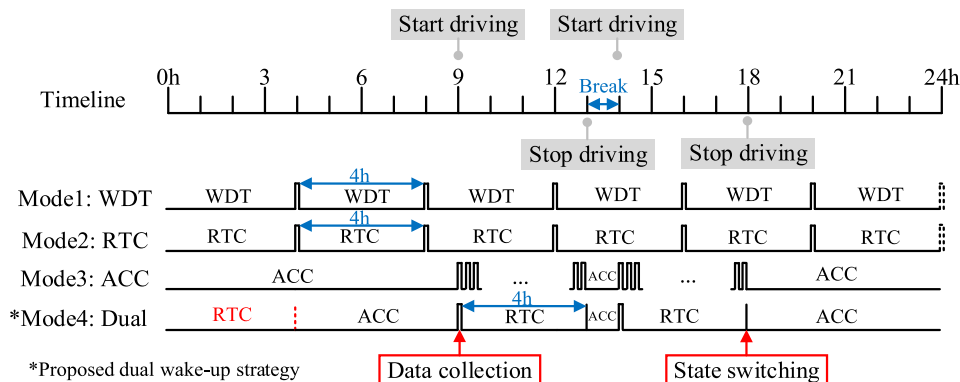
Data starts to be collected and transmitted. Mode 4 is the proposed dual wake-up strategy described in Section 2. The countdown time is set as 4 h and the acceleration threshold is set as the same as Mode 3. The narrow pulses represent the data acquisition and transmission process. A separate vertical line represents state switching from RTC enabled to ACC enabled. Once the cycle starts, the first RTC with red colour in Mode4 will disappear. Because after enabling the accelerometer, it will not trigger until the vehicle speed reaches the set threshold after 9:00 the next day.

For Mode 1 and Mode 2, approximately 6 datasets are collected every day. However, at most two sets of data are valid. Although there is also a slight probability that, on a given day, no data meets the criteria because the vehicle speed is too low or even zero when the data is collected. For Mode 3, since the vehicle speed suit the conditions of triggering the accelerometer after the vehicle starts, the data collection process will always repeat until the vehicle stops. However, only two valid datasets will be collected in 24 h with the proposed dual wake-up strategy in Mode 4. This not only reduces power consumption but also guarantees the validity of the collected data.

After calculation, a 1000mAh battery with a nominal voltage of 3.7 V can support the sensor node to work for about 89 days (Mode 1), 82 days (Mode 2), 22 days (Mode 3) and 1739 days (Mode 4) in these four different working modes, respectively. It further proves the effectiveness and practicality of the proposed dual wake-up strategy.

4. Experiment: Adaptive online sensor Self-Calibration

Because of the manufacturing errors of MEMS components and environmental influence, the measurement accuracy of MEMS sensors is susceptible, which increases the measurement uncertainty of the designed WAWMS. In addition, the dynamics of the vehicle system can be affected by uncertain factors [28] and this, therefore, requires more accurate measurements. Hence, we investigated an adaptive online self-calibration method of the IMU sensor to improve its accuracy and performance in vibration measurement.

4.1. Experimental setup

The IMU calibration tests were carried out on a shaker test rig. As Fig. 10 shows, two IMU sensors and one traditional high-performance integrated electronics piezoelectric (IEPE) accelerometer were installed on the surface of the shaker. The signal generator generated sinusoidal signals with a frequency from 25 Hz to 450 Hz in steps of 25 Hz, respectively. The specifications of these two types of sensors are listed in Table 3.

The IEPE accelerometer recorded 10 s data at a sampling frequency of 96 kHz, whereas the IMUs recorded 400 data packets of acceleration signals at a sampling frequency of 952 Hz. Each data packet has 24 samples for the three axes so the recording period is about 10 s. The
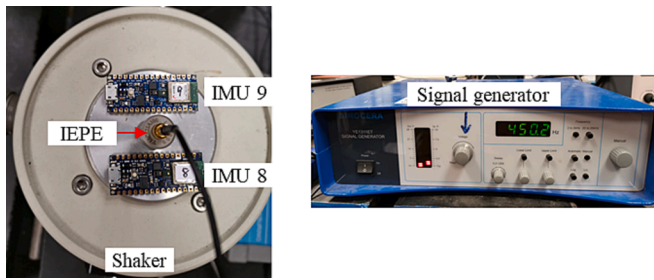

Fig. 9. A 24-hour timeline of four working modes.

Fig. 10. Shaker test rig.

Table 3
Specifications of the sensors.

Parameters	Sensor Type	
	IMU	IEPE
Sample Rate	952 Hz	96 kHz
Range	±16 g	−10 ~ 10 V (50 g)
Sensitivity	0.732 mg/LSB	10.41 mV/(m/s²)
Record Period	About 10 s	10 s

duration of each data packet collected is recorded by the internal RTC, stored at the end of the data packet, and sent to the central device along with the acceleration samples. The recorded time durations are applied to implement the adaptive self-calibration of the sampling frequency of the IMU sensor.

4.2. Uncertainty of sampling frequency

With the shaker test rig, the acquired sinusoidal waveforms of 25 Hz are plotted in Fig. 11 with the DC signal filtered. The signal acquired by the high-performance IEPE accelerometer is regarded as the baseline to compare with those collected by the IMU sensors. Although the sampling frequency of the IMU sensors is not comparable to the IEPE accelerometer, the waveforms still have excellent observability. However, when their spectra are transformed by the sampling frequency of 952 Hz, the drawback of the IMU sensors is uncovered, revealing that the actual sampling frequency of the MEMS sensor is uncertain. Fig. 12 depicts the transformed spectra and frequency errors compared with the IEPE accelerometer. Using the two same IMU sensors, the actual sampling frequency of the IMU8 is lower than 952 Hz, while the IMU9 is higher than 952 Hz. The observed frequency error is around ± 1 % compared with the IEPE accelerometer which further demonstrates the uncertainty of the MEMS sensors and the importance of adaptive online self-calibration. The amplitudes of the spectra are affected by spectral leakage, especially in the high-frequency band. But it has been calibrated by gravity before the tests.

4.3. Proposed sensor Self-Calibration method and validation

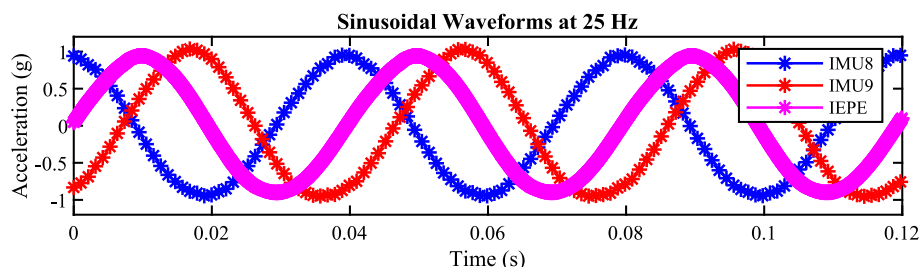An adaptive online self-calibration method was proposed according
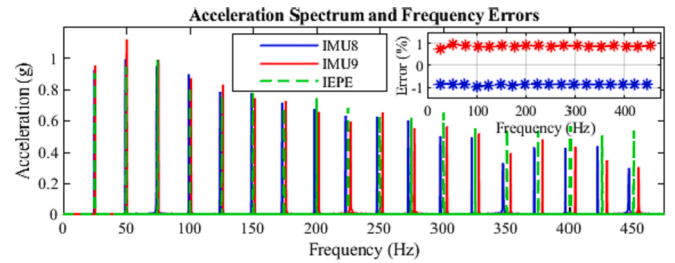
to the real-time measurement of the acquisition duration of each data packet. The raw time durations are displayed with the blue star line in Fig. 13. It is apparent that the first several points have big errors. To determine the probability distribution of the recorded time durations, a large number of experiments were performed to obtain 30,000 samples of time duration. The distribution of these data points is shown in Fig. 14.

As the parametric distribution is not properly described in the histogram, the probability density function (PDF) of the recorded time duration is represented by a kernel distribution fitted with a red dotted line in Fig. 14. The fitting result is a multimodal distribution [29]. Simultaneously, a Gaussian distribution is fitted with a magenta line. The means $\mu_i (i = 0, 1, 2)$ and variances $\sigma_i (i = 0, 1, 2)$ of the raw time duration variables, the fitted multimodal distribution and the Gaussian distribution are calculated and shown in Fig. 14, respectively. The calculated means and variances are similar. With the 2σ rule, approximately 95 % of the population lies within two standard deviations of the mean. Accordingly, a range of $[\mu_0 - 2\sigma_0, \mu_0 + 2\sigma_0]$ is indicated with the green dashed lines to select the 95 % of the time duration samples for frequency calibration. The samples meeting the 2σ rule are selected and marked in red stars in Fig. 13.

The effects of the frequency calibration using both the recorded raw time durations and the 2σ selected values are compared. The frequency errors compared with the baseline after calibration are estimated in Fig. 15. If the calibration is carried out with the raw time durations, the frequency error is only reduced to the range of [0.51%, 0.60%] and [0.42%, 0.62%] for the IMU8 and IMU9, respectively. But with the selected time durations, the frequency errors further decrease to a range of [0.05%, 0.16%] and [− 0.04%, 0.16%] for these two IMU sensors.
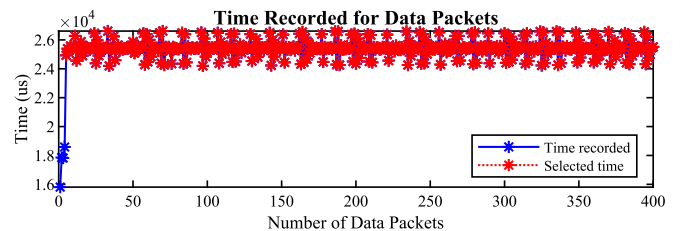

Fig. 12. Spectra and frequency errors compared with the IEPE accelerometer.

Fig. 13. Recorded and selected time duration for data packets.

Fig. 11. Sinusoidal waveforms at 25 Hz by different types of accelerometers.
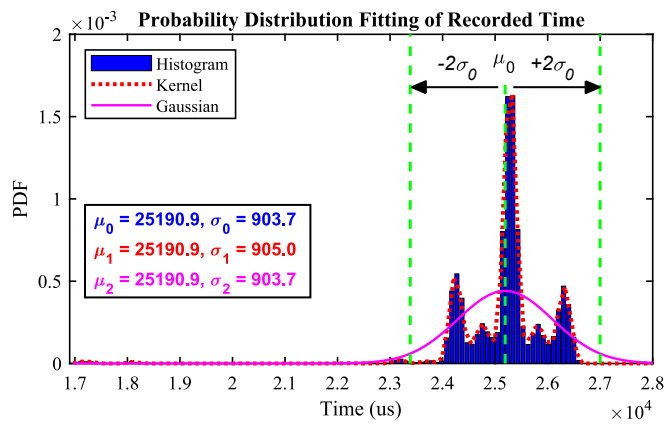
Fig. 14. Probability distribution fitting of recorded time duration.

Therefore, the frequency calibration results with the time durations selected by the 2σ rule are much closer to the IEPE results.

This validates that the proposed method is significantly effective and efficient for the adaptive online calibration of the sampling frequency of the IMU sensor in real time. The frequency error decreases from about 1 % to less than 0.16 %. With the frequency calibration, even if the alignment conditions are classified incorrectly, it can be ruled out that it is caused by measurement errors.

5. Experiment: Real-World validation

5.1. Experimental setup

To verify the effectiveness of the designed WAWMS, we conducted some real-world wheel misalignment field tests with a Ford van. The positive toe, also known as toe-in, is the front of the wheel pointing towards the centre line of the vehicle in the moving forward direction. Conversely, the negative toe, i.e. toe-out, points away from the centre line of the vehicle as displayed in Fig. 16 (a). The toe angles severely affect directional control, steering response and tire tread life. To verify the performance of WAWMS, five different toe alignment angles were adjusted for tests: $-2°$ (toe-out 2°), $-1°$ (toe-out 1°), $0°$ (normal), $1°$ (toe-in 1°) and $2°$ (toe-in 2°). Because the homogeneous characteristics of the wheel and similar broad-band road excitation, only one sensor was installed in a wheel to minimise the costs. The sensor housed in a 3D printed box was installed on the surface of the wheel hub cap as shown in Fig. 16 (b). The distance between the wheel centre and the IMU sensor is about 18 cm. From the official database, the rolling tire circumference is 1991 mm for the van used for the field tests.

For the tests, the driver drove the van at relatively stable speed increments, including 10 mph, 15 mph, 20 mph, 25 mph and 30 mph, for

five wheel alignment scenarios, respectively. The experiments were conducted by four sensors across multiple days and at various locations around Basingstoke, UK. A total of 250 sets of acceleration data were selected at five different speeds for each alignment angle. Overall, the total data obtained is 1250 sets to validate the effectiveness and efficiency of the designed WAWMS. The gyroscope and magnetic data will be investigated in the future. The length of each axis (x-, y-, and z-axis) for each dataset is 4800, with the set acceleration sampling frequency of 952 Hz, that is, the acquisition duration is about 5 s. The real sampling frequency can be calibrated according to the proposed self-calibration method.

5.2. Classification method

Because of the complicated suspension construction of a vehicle, its effective dynamic features related to toe angle changes are difficult to extract. Therefore, a multi-class classifier will be applied to achieve alignment condition classification to validate the effectiveness of the collected acceleration signals by the designed WAWMS.

Fig. 17 shows the diagram of the signal processing method. As introduced in the previous subsection, the initial matrix dimensions of the raw datasets are 1250 (samples) × 4800(features) × 3(axis). Although the driver was asked to carefully control the van speed, most datasets were collected at slightly varying speeds due to the nature of the van operation. Hence, the time waveform of each axis is evenly divided into five non-overlapping segments, which are regarded as five new samples of length 960, about 1 s. The new matrix dimensionality is reshaped as 6250 × 960 × 3. Furthermore, very low and high frequencies are cut off with a band-pass filter to eliminate the influence of ambient noise and potential aliasing Then, the FFT is applied to extract the spectral features. Because the FFT data is symmetrical, only half of them need to be preserved to reduce the matrix dimension to 6250 × 480 × 3. It is followed by reshaping the matrix to 6250 × 1440. It is significant that the features are redundant and have relatively high dimensionality. Principal component analysis (PCA) is a conventional
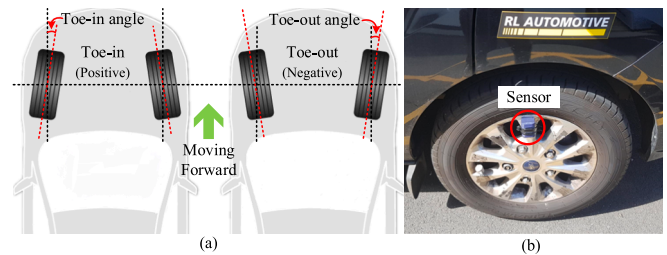

Fig. 16. Toe alignment angles and sensor installation: (a) toe angle drawings, and (b) sensor installation.
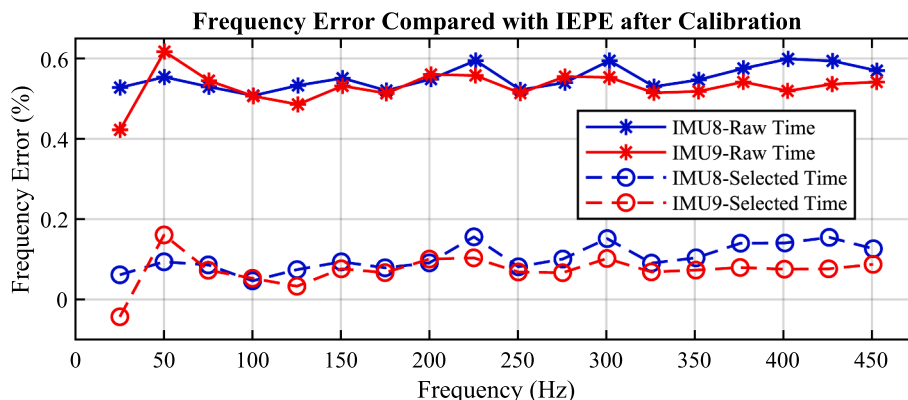

Fig. 15. Frequency error compared with the IEPE accelerometer after calibration.
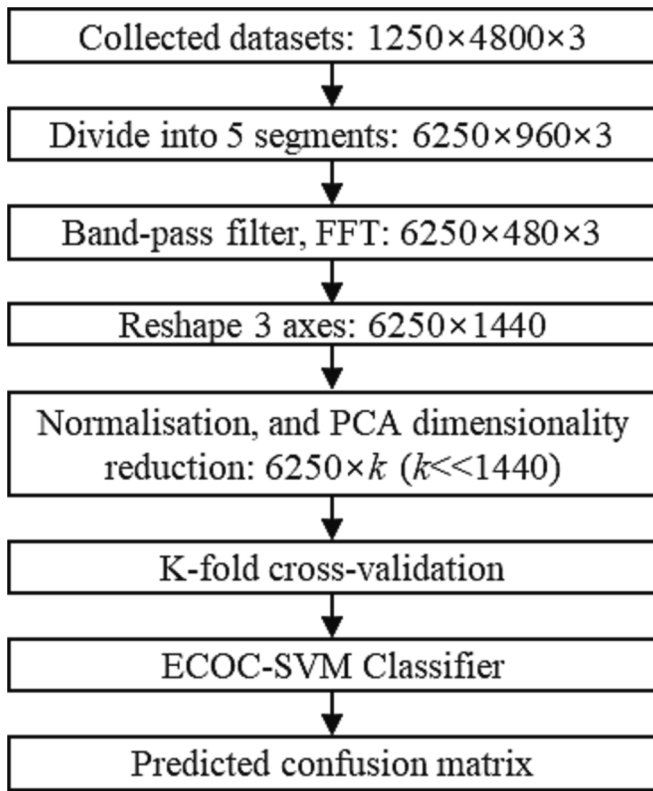
Fig. 17. Diagram of the classification method.

technique to reduce the dimensionality of features and preserve the key principal components of the data through a linear transformation. Therefore, the dimensionality of the normalised features can be reduced from 1440 to k ($k \ll 1440$) with PCA, which means the total acceleration features extracted from all samples are $6250 \times k$. SVMs are powerful supervised machine learning models but are mainly used for binary classification. For a multi-class classification task, SVM can be combined with the ECOC technique because ECOC can convert a multi-class classification problem into a binary classification issue through encoding and error correcting. The ECOC-SVM [30,31] algorithm supported by MATLAB is applied to perform the five classes classification in this study. To validate the trained model, a K-fold cross-validation method is utilised. Finally, a confusion matrix will be calculated to predict the occurrence of each wheel alignment condition.

5.3. Results and discussion

The time waveforms of a 9-DOF IMU are shown in Fig. 18. The acceleration measured by the accelerometer shows strong periodicity which is the oscillation of the gravity with the rotating of the wheel because the MEMS accelerometer can measure DC acceleration. The angular velocity measured by the gyroscope is the rotating speed of the wheels and it can be used for calculating the instantaneous vehicle speed. The magnetic signal describes the magnetic field variation during the rotating of the sensor, which is useful for extracting the angular displacement of the wheel. However, the 3-axis acceleration signals are informative and then only acceleration signals are employed in this validation study. The gyroscope and magnetic signals will be investigated in the future.

To compare the signals at different wheel alignment conditions, both the time waveforms and the spectrums are displayed in Fig. 19. Fig. 19 (a) to (e) present the temporal and spectral characteristics of healthy, toe-in 1°, toe-in 2°, toe-out 1°, and toe-out 2°, respectively. The time waveforms look similar and are difficult to distinguish visually. The corresponding spectra of the five cases show some differences, especially around 270 Hz. The amplitude at around 270 Hz increases with the misalignment of both toe-in and toe-out. Although there are some
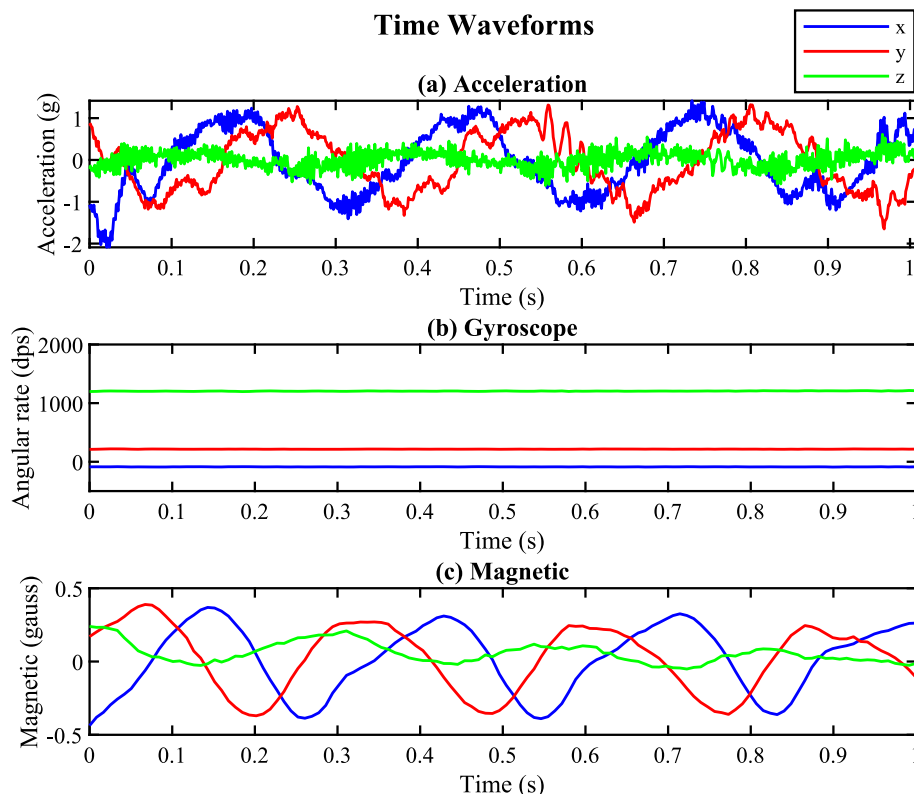

Fig. 18. Time waveforms at 15 mph van speed: (a) acceleration, (b) gyroscope, and (c) magnetic.
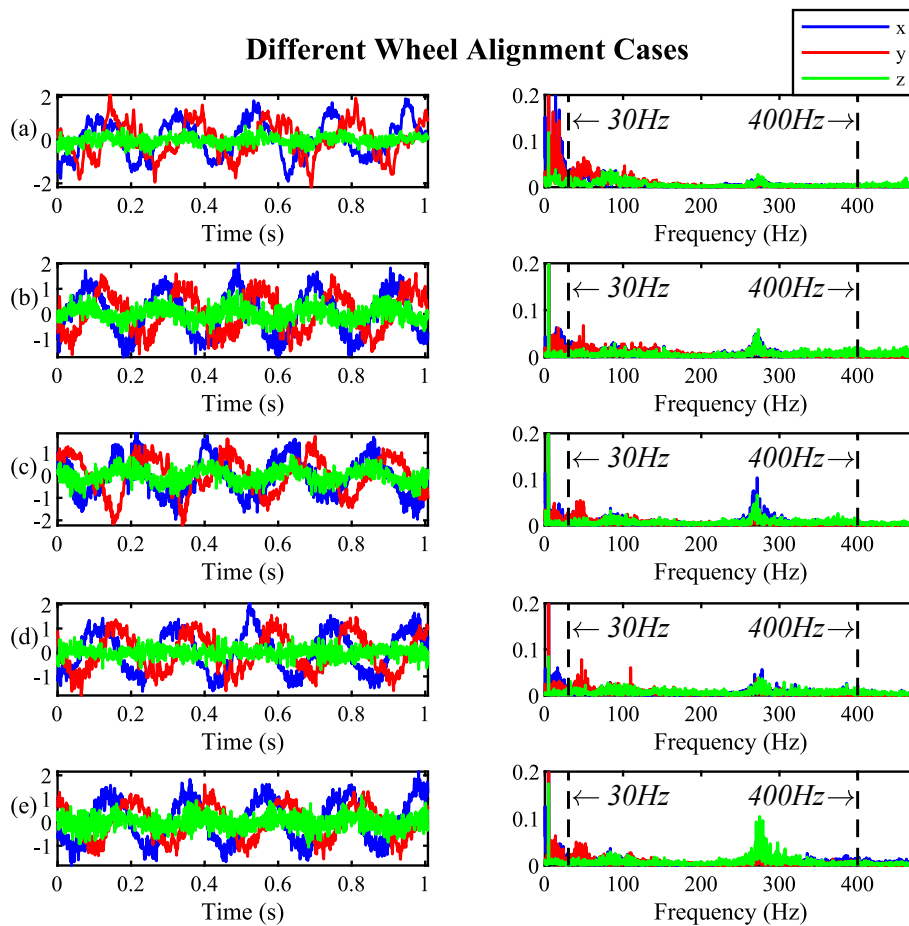
Fig. 19. Acceleration waveform and spectrum of different alignment conditions at 20 mph: (a) Healthy, (b) Toe-in 1', (c) Toe-in 2', (d) Toe-out 1', and (e) Toe-out 2'.

characteristics in the spectra, it is still hard to distinguish different wheel alignment conditions via human observation because characteristic changes caused by wheel misalignment are ambiguous. Therefore, a multi-class classifier based on ECOC and SVM is applied to categorise the extracted features into five classes. As the vibration in the low frequency is usually noisy, the frequency band from 30 Hz to 400 Hz is selected for the feature extraction.

As described in Section 5.2, the dimensionality of the normalised features will be reduced to k through PCA. The choice of k value has a direct impact on the classification results. Therefore, the weights of eigenvalues for the first 30 PCs are displayed in Fig. 20 (a). It can be seen that the first few PCs have no absolutely high proportion. The weight decreases gently from the sixth PC. The traditional 95 % of the total variance to determine k does not work well in this study. As a result, the SVM results were used to compare the optimal k value. The value of k was set from 1 to 20 to reduce the feature dimension, respectively. A 5-fold cross-validation method was applied to divide all dimensionality-reduced features into 5 sets, one of which was used as test data and the other four as training data. A Gaussian kernel was selected as the kernel function of SVM in this study. The means and standard deviations of SVM results under different k values are shown in Fig. 20 (b). The mean value increases to the peak of 93.2 % at $k = 9$ then falls with the increase of k values. Therefore, the first 9 PCs were selected as the features for different alignment angle classification in this research.

The predicted results are shown with a confusion matrix in Fig. 21. Obviously, the discrimination of these five alignment angles can reach above 90 %. The average classification accuracy and the standard deviation are 93.2 % and 1.28 %, respectively.

Consequently, the classification results can demonstrate the effectiveness of the designed WAWMS for automotive wheel alignment
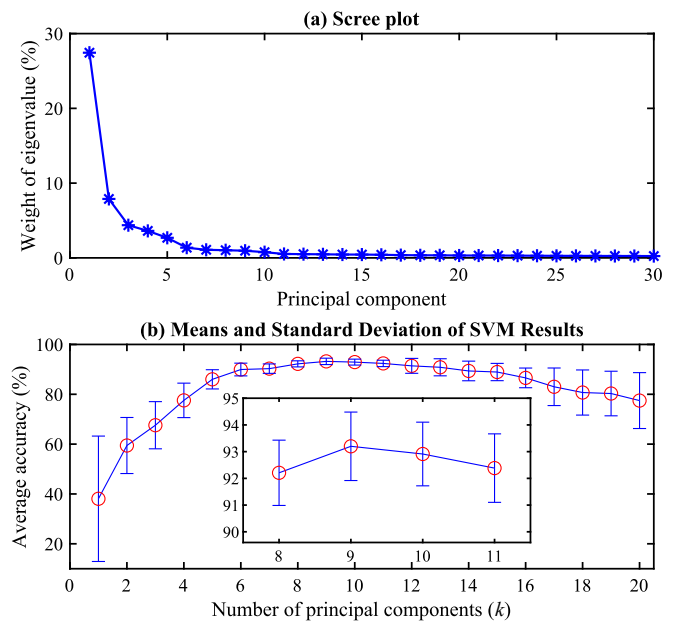

Fig. 20. Selection of principal components.

monitoring. An advanced machine learning approach is being developed from the cloud server to achieve accurate and reliable real-time condition monitoring of wheel alignment for different types of vehicles and roads, and various loading and operating conditions with 9-DOF

Classification Accuracy

Predicted Class	Healthy	Toe-in 1°	Toe-in 2°	Toe-out 1°	Toe-out 2°
Healthy	1158	52	3	4	10
Toe-in 1°	75	1161	31	38	56
Toe-in 2°	6	13	1183	12	25
Toe-out 1°	5	12	11	1179	15
Toe-out 2°	6	12	22	17	1144
	92.6%	92.9%	94.6%	94.3%	91.5%
	7.4%	7.1%	5.4%	5.7%	8.5%
	Healthy	Toe-in 1°	Toe-in 2°	Toe-out 1°	Toe-out 2°

True Class

Fig. 21. Confusion matrix for different alignment conditions using SVM.

measurements. The accurate wheel alignment monitoring will promisingly decrease unnecessary tyre wear and reduce environmental pollution, especially microplastics.

6. Conclusions

In this paper, an energy-efficient onboard WAWMS is developed to monitor automotive wheel alignment conditions. It was fabricated using the selected low-power and low-cost components. Additionally, a dual wake-up strategy is proposed, which can not only reduce the power consumption of the system but can also make the system more suitable for practical applications. Its current consumption is reduced to 9.13μA which prolongs the service life of a 1000mAh battery up to 1739 days. This makes WAWMS a promising future-proof solution as a fully autonomous self-sustaining sensing system especially after embedding energy harvesting technology into the design. The design includes a data packet time duration based online self-calibration method to adaptively calibrate the IMU sampling frequency to reduce the measurement uncertainty and improve sensor accuracy. The sampling frequency error decreases from approximately 1 % to less than 0.16 %. Finally, five different alignment angles can be identified by the ECOC-SVM method to implement an average accuracy of 93.2 %, which verifies the effectiveness and efficiency of the designed WAWMS.

Compared with traditional wheel alignment equipment, this designed WAWMS is economical, convenient and smart. Since the designed WAWMS contains the IMU and the pressure and temperature sensor, it has the potential to substitute conventional TPMS equipment. Therefore, WAWMS will contribute to the extension of the automotive service life, improvement of stability and safety of vehicle handling, and reduction of vehicle maintenance costs. It can also be applied to other rotating machinery monitoring fields.

To accurately monitor the wheel alignment conditions of many vans and cars in real time, an advanced deep learning method will be developed to run on a cloud platform in the future. Additionally, the dynamics of the wheel system will be studied to give an insightful understanding of the influence of wheel misalignment. Therefore, the findings can support the optimisation of the installation of the wireless wheel alignment monitoring system, and the feature extraction for effective automotive alignment monitoring.

CRediT authorship contribution statement

Xiaoli Tang: Conceptualization, Methodology, Investigation. **Yu Shi:** Conceptualization, Supervision. **Boyue Chen:** Validation. **Mark Longden:** Funding acquisition, Project administration. **Rabiya Farooq:** Software, Data curation. **Harry Lees:** Software, Data curation. **Yu Jia:** Funding acquisition, Conceptualization, Supervision.

Declaration of Competing Interest

The authors declare that they have no known competing financial interests or personal relationships that could have appeared to influence the work reported in this paper.

Data availability

The data that has been used is confidential.

Acknowledgements

References

[1] G. D'Mello, R. Gomes, R. Mascarenhas, S. Ballal, V.S. Kamath, V.J. Lobo, Wheel alignment detection with IoT embedded system, Mater. Today Proc. (Dec. 2021), https://doi.org/10.1016/j.matpr.2021.11.566.

[2] D. Wei, et al., Multiple limit-cycles shimmy characteristics of dual-axle steering mechanism considering the wheel alignment parameters, Proc. Inst. Mech. Eng. Part C J. Mech. Eng. Sci. 234 (17) (Sep. 2020) 3360–3379, https://doi.org/10.1177/0954406220915499.

[3] J.-S. Young, H.-Y. Hsu, C.-Y. Chuang, Camber Angle Inspection for Vehicle Wheel Alignments, Sensors 17 (2) (Feb. 2017) 285, https://doi.org/10.3390/s17020285.

[4] H. Patel et al., 'Suspension Variables Influencing Static Vehicle Wheel Alignment Measurements', SAE Int. J. Passeng. Cars - Mech. Syst., vol. 9, no. 2, Art. no. 2016-01–1571, Apr. 2016, doi: 10.4271/2016-01-1571.

[5] R. Furferi, L. Governi, Y. Volpe, M. Carfagni, Design and Assessment of a Machine Vision System for Automatic Vehicle Wheel Alignment, Int. J. Adv. Robot. Syst. 10 (5) (May 2013) 242, https://doi.org/10.5772/55928.

[6] A. Padegaonkar, M. Brahme, M. Bangale, A.N.J. Raj, Implementation of Machine Vision System for Finding Defects in Wheel Alignment, Int. J. Comput. Technol. 1 (7) (Aug. 2014) 6.

[7] C.-H. Shao, S.-S. Xu, Y. Song, Z.-Y. Zhang, Q.-X. Zhang, Methods of automatic calibration for four-wheel alignment based on superimposing angles, Int. J. Veh. Des. 81 (2019) 14.

[8] C.-H. Shao, Z.-Y. Zhang, S.-S. Xu, Q.-X. Zhang, Calibration point distribution study of a four-wheel alignment optimization device based on a blanket technology algorithm, Rev. Sci. Instrum. 91 (4) (Apr. 2020), 044102, https://doi.org/10.1063/1.5144492.

[9] S.H. Kim, K.I. Lee, Wheel Alignment of a Suspension Module Unit Using a Laser Module, Sensors 20 (6) (Mar. 2020), https://doi.org/10.3390/s20061648.

[10] Z. Niu, S. Jin, Z. Li, Assembly Variation Analysis of Incompletely Positioned Macpherson Suspension Systems Considering Vehicle Load Change, J. Mech. Des. 143 (5) (May 2021), 052001, https://doi.org/10.1115/1.4048413.

[11] J. Yunta, D. Garcia-Pozuelo, V. Diaz, O. Olatunbosun, Influence of camber angle on tire tread behavior by an on-board strain-based system for intelligent tires, Measurement 145 (Oct. 2019) 631–639, https://doi.org/10.1016/j.measurement.2019.05.105.

[12] S. Chatur, Computer based Wireless Automobile Wheel Alignment system using Accelerometer, Int. J. Eng. Sci. 4 (9) (Sep. 2015) 62–69.

[13] Y.G. Cho, Static and dynamic wheel alignment analysis of steering drift under straight braking, Int. J. Veh. Des. vol. 56, no. 1/2/3/4 (2011) 4, https://doi.org/10.1504/IJVD.2011.043270.

[14] M. Danek and I. Kousari, 'AUTOMOTIVE WHEEL ALIGNMENT SYSTEM', University of Illinois Urbana-Champaign, Dec. 2016. [Online]. Available: https://courses.engr.illinois.edu/ece445/getfile.asp?id=8679.

[15] J.-S. Young, H.-Y. Hsu, Toe Angle Measurement for z-Axis Calibrations of the Toe Sensor Based on MCU, Int. J. Electron. Electr. Eng. 6 (4) (2018) 61–64, https://doi.org/10.18178/ijeee.6.4.61-64.

[16] Y. Liu, G. Yang, Y. Liu, X. Li, and Y. Zhang, 'Research and Implementation of Digital Two-dimensional Inclination Measurement System', in 2020 39th Chinese Control Conference (CCC), Jul. 2020, pp. 3631–3635. doi: 10.23919/CCC50068.2020.9188618.

[17] S. Paudel, A. M. H. S. Abeykoon, and S. D. A. P. Senadeera, 'Sensor-Less Detection of Wheel Alignment Error for a Wheeled Mobile Robot using the Disturbance Observer', in 2020 Moratuwa Engineering Research Conference (MERCon), Jul. 2020, pp. 572–577. doi: 10.1109/MERCon50084.2020.9185394.

[18] M.H. Sulaiman, S. Sulaiman, A. Saparon, IoT for wheel alignment monitoring system, Int. J. Electr. Comput. Eng. IJECE 11 (5) (Oct. 2021) 3809, https://doi.org/10.11591/ijece.v11i5.pp3809-3817.

[19] X. Tang *et al.*, 'Towards Power Neutral Wireless Sensors: a Real-Time Wheel Alignment Monitoring System', in *2021 IEEE 20th International Conference on Micro and Nanotechnology for Power Generation and Energy Conversion Applications (PowerMEMS)*, Dec. 2021, pp. 124–127. doi: 10.1109/PowerMEMS54003.2021.9658408.

[20] Y. Jia, Review of nonlinear vibration energy harvesting: Duffing, bistability, parametric, stochastic and others, J. Intell. Mater. Syst. Struct. 31 (7) (Apr. 2020) 921–944, https://doi.org/10.1177/1045389X20905989.

[21] X. Tang, X. Wang, R. Cattley, F. Gu, A.D. Ball, Energy Harvesting Technologies for Achieving Self-Powered Wireless Sensor Networks in Machine Condition Monitoring: A Review, Sensors 18 (12) (Dec. 2018) 4113, https://doi.org/10.3390/s18124113.

[22] L. Xie, S. Cai, G. Huang, L. Huang, J. Li, X. Li, On Energy Harvesting From a Vehicle Damper, IEEEASME Trans. Mechatron. 25 (1) (Feb. 2020) 108–117, https://doi.org/10.1109/TMECH.2019.2950952.

[23] Y. Xu, et al., Orthogonal On-Rotor Sensing Vibrations for Condition Monitoring of Rotating Machines, J. Dyn. Monit. Diagn. (Dec. 2021), https://doi.org/10.37965/jdmd.v2i2.47.

[24] R. Kanan, O. Elhassan, R. Bensalem, An IoT-based autonomous system for workers' safety in construction sites with real-time alarming, monitoring, and positioning

[25] strategies, Autom. Constr. 88 (Apr. 2018) 73–86, https://doi.org/10.1016/j.autcon.2017.12.033.

[25] M. Giordano, N. Baumann, M. Crabolu, R. Fischer, G. Bellusci, and M. Magno, 'Design and Performance Evaluation of an Ultra Low-Power Smart IoT Device with Embedded TinyML for Asset Activity Monitoring', p. 11.

[26] F. Kiani, Animal behavior management by energy-efficient wireless sensor networks, Comput. Electron. Agric. 151 (Aug. 2018) 478–484, https://doi.org/10.1016/j.compag.2018.06.046.

[27] R. Ballestrin, R. Bender, V. Brusamarello, and I. Müller, 'Low cost wireless sensor network for vibration detection', in *2017 2nd International Symposium on Instrumentation Systems, Circuits and Transducers (INSCIT)*, Aug. 2017, pp. 1–6. doi: 10.1109/INSCIT.2017.8103518.

[28] C. Fu, Y. Xu, Y. Yang, K. Lu, F. Gu, A. Ball, Response analysis of an accelerating unbalanced rotating system with both random and interval variables, J. Sound Vib. 466 (Feb. 2020), 115047, https://doi.org/10.1016/j.jsv.2019.115047.

[29] O. Kesemen, B. K. TiRyakï, E. Özkul, and Ö. Tezel, 'Determination of the Confidence Intervals for Multimodal Probability Density Functions', p. 18, 2018.

[30] J. Shi, et al., Fault diagnosis in a hydraulic directional valve using a two-stage multi-sensor information fusion, Measurement 179 (Jul. 2021), 109460, https://doi.org/10.1016/j.measurement.2021.109460.

[31] Z. Qiu, R. Min, D. Wang, S. Fan, Energy features fusion based hydraulic cylinder seal wear and internal leakage fault diagnosis method, Measurement 195 (May 2022), 111042, https://doi.org/10.1016/j.measurement.2022.111042.